Journal of Quantitative Spectroscopy & Radiative Transfer 112 (2011) 980–989

Contents lists available at ScienceDirect

Journal of Quantitative Spectroscopy & Radiative Transfer

journal homepage: www.elsevier.com/locate/jqsrt

An efficient analytical approach for calculating line mixing in atmospheric remote sensing applications

Chris D. Boone [a,*], Kaley A. Walker [a,b], Peter F. Bernath [a,c]

[a] Department of Chemistry, University of Waterloo, Waterloo, Ontario, Canada N2L 3G1
[b] Department of Physics, University of Toronto, Toronto, Ontario, Canada M5S 1A7
[c] Department of Chemistry, University of York, Heslington,York YO10 5DD, UK

ARTICLE INFO

Article history:
Received 29 June 2010
Received in revised form
12 November 2010
Accepted 16 November 2010
Available online 23 November 2010

Keywords:
Line shape
Line mixing
Remote sensing

ABSTRACT

Collisional coupling between energy states in a molecule undergoing an optical transition can alter the line shape associated with the transition, an effect known as line mixing. Accounting for this effect in the analysis of remote sensing measurements of Earth's atmosphere by the Atmospheric Chemistry Experiment (ACE) yields reduced residuals, which leads to improved performance in the volume mixing ratio retrievals for some molecules. Analytical expressions are presented for the imaginary components of the polynomial ratios from the Humlicek algorithm, which provides approximate solutions to the complex probability function. These imaginary components are employed in the calculation of line mixing using the Rosenkranz first order approximation. Examples of line mixing in ACE measurements are presented, including a set of CH_4 lines that exhibit both line mixing and speed dependence. An efficient, analytical approach is proposed for calculating line shapes with a combination of line mixing and speed dependence. FORTRAN routines for calculating line mixing effects are provided as a supplement to the paper.

1. Introduction

Collisionally-induced coupling between energy states in a molecule gives rise to an interference effect in the measurement of optical transitions involving the coupled states. This effect, known as line mixing, has been observed in the infrared spectra of several molecules, including CO_2 [1,2], CH_4 [3–6], H_2O [7], O_3 [8,9], CO [10], N_2O [11], CH_3Cl [12], and CH_3Br [13]. With line mixing, when two or more "coupled" lines (i.e., closely-spaced lines where the initial and final energy states involved in the optical transitions are collisionally coupled) exhibit significant overlap within their pressure broadened (Lorentzian) line shapes, there exists an additional contribution to the homogeneous line shape (i.e., on top of the traditional Lorentzian pressure broadening) [14].

The Atmospheric Chemistry Experiment (ACE), otherwise known as Scisat-1, is a Canadian-led satellite mission for remote sensing of Earth's atmosphere, launched August 2003 into a low-Earth (650 km altitude) circular orbit inclined 74° to the equator [15]. The primary instrument on Scisat-1 is the ACE-FTS, a Fourier transform spectrometer (FTS) featuring high resolution (0.02 cm^{-1}, corresponding to a $\pm$25 cm maximum optical path difference) and broad spectral coverage in the infrared (750–4400 cm^{-1}). The ACE-FTS works primarily in the solar occultation mode, collecting atmospheric limb measurements using the sun as a radiation source.

The current processing version for the ACE-FTS is version 3.0. This processing version provides pressure, temperature, volume mixing ratio (VMR) profiles for 35 molecules plus VMR profiles for more than 20 subsidiary isotopologues. Line mixing is not included in ACE-FTS

* Corresponding author. Tel.: +1 519 888 4814; fax: +1 519 746 0435.
E-mail address: cboone@uwaterloo.ca (C.D. Boone).

0022-4073/$ - see front matter © 2010 Elsevier Ltd. All rights reserved.
doi:10.1016/j.jqsrt.2010.11.013

version 3.0 results but is planned for a future processing version.

Neglecting line mixing in the ACE-FTS spectra has implications for the accuracy of CH_4 retrievals. Perhaps more significantly, though, large residuals from neglecting line mixing in CH_4 can pollute potential microwindows for other molecules. CH_4 features prominently in the infrared measurements collected by the ACE-FTS. With a dense collection of spectral lines in multiple wavenumber regions, CH_4 often serves as an interferer in the VMR retrievals of other molecules. Thus, large fitting residuals from neglecting CH_4 line mixing can impact the retrievals for other molecules.

Significant line mixing effects have been observed in the CH_4 P- and R-branches for both the ν_3 [4,5] and ν_4 [6] bands. Retrievals for the ACE-FTS make use of microwindows: small portions of the spectrum (typically around 0.5 cm^{-1} wide) containing a spectral feature (or multiple spectral features) from the target molecule, ideally with minimal interferences from other molecules. In ACE-FTS version 3.0 (and earlier) processing, there are several molecules featuring microwindows within the wavenumber ranges spanned by the ν_3 and ν_4 bands of CH_4, including N_2O, H_2O_2, HCN, N_2O_5, CF_4, $ClONO_2$, NO_2, H_2CO, HCl, CH_3Cl, and H_2O. It is not clear at this time how much of an effect CH_4 line mixing has on the retrieval quality for any of these molecules. The microwindow selection process used fitting residuals as a filter. Discarding potential microwindows with large fitting residuals minimizes line mixing effects to a degree but certainly provides no guarantee of avoiding the effects altogether. In some cases (e.g., H_2CO and NO_2 at low altitudes), avoiding large residuals severely limits the number of available microwindows, which will affect the quality of the retrieval.

For larger molecules with broad spectral features (such as N_2O_5, $ClONO_2$, and CF_4), it is not possible to pick and choose microwindows with the best residuals to minimize line mixing effects. These molecules often have a single spectral feature in a given region. If there are CH_4 lines suffering from line mixing overlapping these broad spectral features, then you cannot simply discard the microwindow and choose another, because in some cases no other microwindow is available. You can (1) ignore the line mixing and deal with the possibility of increased retrieval errors, (2) give reduced weights in the fitting process to regions where you expect significant line mixing effects in order to reduce the impact on the retrieval, or (3) explicitly account for line mixing in your forward model calculations.

Neglecting CH_4 line mixing could also make it more challenging to generate retrievals for molecules with weak spectral signatures in the infrared, such as SO_2 or HOCl. Also, around 2950 cm^{-1} (within the CH_4 ν_3 band), one might expect to see weak C–H stretch features from a number of molecules (e.g., propane), but it may not be possible to distinguish some of these features without first accounting for line mixing in CH_4.

Line mixing for molecules other than CH_4 has implications in the analysis of ACE-FTS spectra. For example, line mixing in a CO_2 Q-branch near 790 cm^{-1} affects the retrieval of CCl_4 (as discussed later in this paper), and line mixing in a Q-branch of N_2O near 2800 cm^{-1} [11] ruins a potential microwindow for H_2CO. However, it is the presence of significant line mixing in P- and R-branches of CH_4 that generates widespread line mixing effects in ACE-FTS spectra. Possible line mixing effects in CO_2 P- and R-branches [2] are not as obvious as line mixing effects in CH_4 for ACE-FTS spectra but may play some role in retrieval accuracies.

Accounting for line mixing in the ACE-FTS analysis will improve results for several molecules in the current dataset. It will also hopefully open up possibilities for adding new molecules, i.e., weak absorbers with spectral signatures currently obscured by large residuals from neglecting line mixing.

Processing time in the analysis of ACE-FTS data is a major concern, as it would be for any atmospheric remote sensing mission that generates a large number of measurements. Line mixing calculation approaches that strive to achieve the greatest possible accuracy (see, e.g., Pine and Gabard [5] or Smith et al. [6]) tend to have cumbersome computational requirements and are not well suited to the line-by-line calculation approach often used in atmospheric remote sensing applications. Highly accurate line mixing calculations are generally not required for the ACE-FTS. The primary impetus for including line mixing in ACE-FTS analysis is to reduce fitting residuals in situations where the molecule suffering from line mixing is not the "target" molecule.

The line mixing calculation approach described in this paper is efficient, in part because it avoids the use of complex variables. It is an analytical approach, facilitating the calculation of analytical derivatives of the line shape with respect to fitting parameters. It provides reasonably accurate results over the range of conditions encountered in Earth's stratosphere and upper troposphere, and it is compatible with a line-by-line calculation approach.

2. Calculations

In the analysis of infrared atmospheric measurements, the line shape is typically taken as a Voigt function, which is a convolution between a Lorentzian line shape (from pressure broadening) and a Gaussian line shape (from Doppler broadening). The Voigt line profile is

$$g_v = \frac{\sqrt{\ln 2/\pi}}{\gamma_D} K(x,y), \tag{1}$$

with the Voigt function defined by

$$K(x,y) = \frac{y}{\pi}\int_{-\infty}^{\infty} \frac{e^{-t^2}}{(x-t)^2+y^2}\,dt, \tag{2}$$

where x and y are the dimensionless variables

$$x = \sqrt{\ln 2}\,\frac{\omega-\omega_o+\eta}{\gamma_D} \text{ and } y = \sqrt{\ln 2}\,\frac{\gamma_L}{\gamma_D}, \tag{3}$$

where $\omega-\omega_o$ is the detuning from line center (with ω_o as the wavenumber at line center in the limit of low pressure, the quantity tabulated in spectroscopic databases such as HITRAN [16]), η is the pressure shift, typically assumed proportional to pressure although in general it should contain a temperature dependence [6], γ_L is the pressure broadening Lorentzian half width, and γ_D is the Doppler

half width defined as

$$\gamma_D = \omega_o \sqrt{\frac{2\ln 2 kT}{mc^2}}, \tag{4}$$

where k is the Boltzmann constant, c is the speed of light, m is average molecular mass, and T is temperature in kelvin.

Combining x and y into the complex variable $z=x+iy$, we can represent the Voigt function $K(x,y)$ as the real part of a complex function $W(z)$

$$K(x,y) = \mathbf{Re}[W(z)] = \mathbf{Re}\left[\frac{i}{\pi}\int_{-\infty}^{+\infty}\frac{e^{-t^2}}{z-t}dt\right]. \tag{5}$$

The benefit of expressing the calculation of the Voigt function in this manner is that for y greater than zero (as it must be), the function $W(z)$ is equal to the complex probability function $w(z)$

$$w(z) = e^{-z^2}\left(1+\frac{2i}{\sqrt{\pi}}\int_0^z e^{t^2}dt\right) = e^{-z^2}\,\mathrm{erfc}(-iz), \tag{6}$$

where erfc( ) is the complementary error function.

The properties of the complex probability function have been extensively studied, and existing strategies for evaluating this function have been exploited to derive efficient algorithms for calculating the Voigt function. Of particular interest is an approach developed by Humlicek [17] where approximate solutions to Eq. (6) are expressed as the ratio of two polynomials. With the Humlicek algorithm, the calculation is divided into different regions governed by the value of $|x|+y$, employing the minimum number of terms in the polynomials to achieve the target accuracy for the given region.

The Humlicek algorithm is derived in terms of the complex variable z, but only the real part of $W(z)$ is required for calculating the Voigt function. A subsequent paper by Kuntz [18] (with the appropriate typographical corrections [19]) provided analytical expressions for calculating the real component of the polynomial ratios from the Humlicek algorithm, avoiding altogether calculation of the imaginary component.

The function $W(z)$ (implicitly defined in Eq. (5)) has an imaginary component of the following form [20]:

$$L(x,y) = \frac{1}{\pi}\int_{-\infty}^{\infty}\frac{(x-t)\exp(-t^2)}{(x-t)^2+y^2}dt. \tag{7}$$

This function has a dispersion shape and can be related to derivatives of the real component of $W(z)$ with respect to x and y [20]. More significantly though (for the purposes of this paper), the imaginary component of $W(z)$ can be employed in the treatment of line mixing through the Rosenkranz [21] first order approximation. With the Rosenkranz first order approximation, the line profile is as follows [1,20]:

$$g_{V,LM} = \frac{\sqrt{\ln 2/\pi}}{\gamma_D}\mathbf{Re}[(1-iY)W(z)] = \frac{\sqrt{\ln 2/\pi}}{\gamma_D}(K(x,y)+YL(x,y)), \tag{8}$$

where Y is the coupling coefficient, and the subscripts V and LM refer to Voigt and line mixing, respectively. The coupling coefficient, Y, is a function of pressure and temperature. Because the variation in Y is driven primarily by the variation of pressure broadening in the overlapping lines, a convenient strategy is to assume the same form used for pressure broadening [3]

$$Y(P,T) = PY_o\left(\frac{T_o}{T}\right)^n, \tag{9}$$

where P is pressure, T is temperature in kelvin, and T_o is a reference temperature (usually taken as 296 K). In principle, the temperature dependence of the line mixing will likely be more complicated than this [1], but the above form is hopefully sufficiently accurate over the relatively limited range of temperatures expected in atmospheric measurements.

Analytical expressions for calculating the imaginary component of the polynomial ratios from the Humlicek algorithm (which represent approximate solutions to $L(x,y)$ in Eq. (7)) are presented in the Appendix of this paper. This represents (to the best of our knowledge) the first time these expressions have been explicitly reported in the literature, although a paper by Wells [22] provided a FORTRAN subroutine that included an analytical calculation of $L(x,y)$ that used expressions equivalent to those reported here, except for Humlicek's "region 4," where a different expression was employed. These analytical expressions for calculating the imaginary component of the complex probability function complement the analytical expressions for calculating the real component provided by Kuntz [18] and Ruyten [19].

3. Examples

Fig. 1 shows ACE-FTS fitting residuals in the vicinity of the P(9) manifold in the ν_3 band of CH_4 with and without line mixing included in the calculation. Ideally, the line mixing parameters for this calculation would be taken from CH_4 laboratory studies. Unfortunately, the compatibility of parameters available in the literature is a problem. Previous CH_4 line mixing studies employed hard-collision line shapes (rather than Voigt) [3,4] or a combination of hard collisions and speed dependence [5]. The hard-collision line shape is not currently available in the ACE-FTS software but will be in the near future. Also, the previous studies used N_2 broadening, but air broadening would have been more appropriate when considering ACE-FTS measurements. Many previous studies [e.g., 4,5] were performed at room temperature, but line mixing parameters are temperature dependent, and the values for Y at atmospheric temperatures could be quite different from those at room temperature. One study [3] investigated the temperature dependence of line mixing parameters within the P(9) manifold but could only measure four of the eight lines within the manifold due to the limited range of their tunable diode laser.

In short, we lack compatible line mixing parameters to use in the calculations for the CH_4 P(9) manifold in Fig. 1. Thus, for this preliminary study, line mixing parameters were fitted from the ACE-FTS spectra using a modified version of the ACE-FTS retrieval software [23]. Line positions and the relative intensities of CH_4 lines within the manifold were also adjusted, although it is possible the need to vary line positions was compensating for the fact that a Voigt line shape was being used in the calculation rather than the more appropriate hard-collision line shape. No improvements to the fitting were achieved from fitting other variables (e.g., pressure broadening, pressure shift),

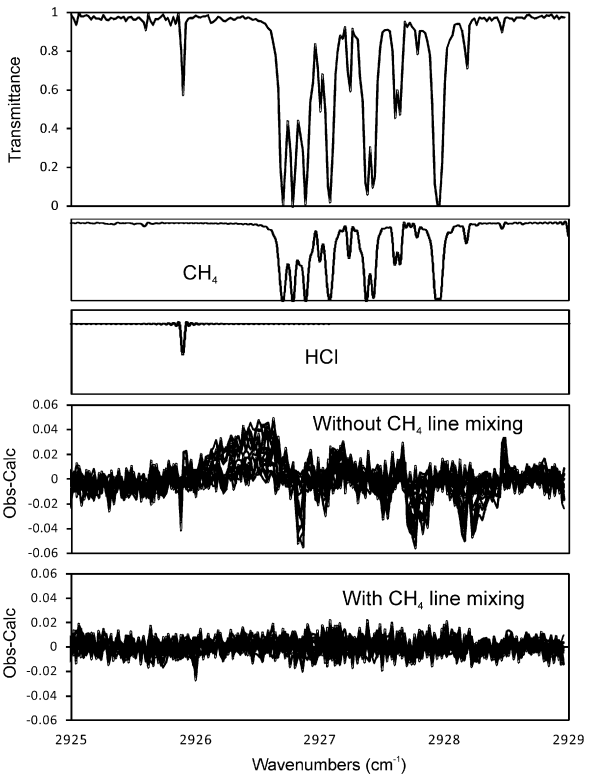

Fig. 1. ACE-FTS spectrum in the vicinity of the P9 manifold in the ν_3 band of CH_4. The top panel shows the measured spectrum near 25 km for ss11613 (latitude 4°S, longitude 108°W, October 9, 2005). The next two panels show the contributions to the spectrum from CH_4 and HCl, respectively. The panel below that has the fitting residuals with line mixing in P9 manifold neglected, where the residuals for all of the measurements in the occultation between 12 and 30 km (a total of 14 measurements) are shown on a common plot. The bottom panel shows the fitting residuals when CH_4 line mixing is taken into account, where the line mixing parameters are determined from least-squares fitting of the ACE-FTS spectra.

and so they were fixed to their values from the HITRAN line list.

For the analysis in Fig. 1, the temperature exponent for the coupling coefficient (n in Eq. (9)) was fixed to the temperature exponent for pressure broadening. The previous investigation into temperature dependences within the P(9) manifold [3] noted that the temperature exponents for pressure broadening and line mixing are quite different. However, the range of temperatures in the ACE-FTS spectra was insufficient to accurately determine temperature dependences for the line mixing parameters. It should be stressed that the parameters derived from this preliminary study are not intended to be used in subsequent analysis. A more accurate determination of line mixing parameters awaits a forthcoming study of CH_4 laboratory spectra. There is a general, rough agreement between the line mixing parameters determined through least-squares fitting of the ACE-FTS spectra and results published previously in the literature, but, again, with the differences in assumed line shape and temperature dependence (or lack thereof for some studies), one would not expect close agreement.

As indicated in Fig. 1, there is an HCl line close to the P(9) manifold. When line mixing is not included in the calculation, the apparent baseline in the vicinity of the HCl line is not symmetric about line center. This could introduce errors in the retrieval process if care is not taken. Note the increased residuals associated with the HCl line when the CH_4 line mixing is not taken into account. This is due in part to a misalignment of the measured and calculated spectra. ACE-FTS spectra lack accurate wavenumber calibration. To address this problem, a frequency offset between the measured and calculated spectra is determined by taking a cross correlation of the two spectra. When the shapes of the measured and calculated spectra differ (due, e.g., to neglecting line mixing in the calculated spectra), one can get an error in the calculated offset.

In ACE-FTS version 3.0 (and earlier) processing, the microwindows for some HCl lines were limited to higher altitudes in order to avoid significant pollution from neglected CH_4 line mixing. There are a relatively small number of HCl lines available in the ACE-FTS spectral range, and reducing the number of HCl microwindows employed at a particular altitude could have a noticeable effect on retrieval precision. This is an example of an "indirect effect" of line mixing on retrievals. For molecules with a relatively scarce number of potential microwindows (e.g., HCl, H_2CO, low altitude NO_2,…), discarding a microwindow in order to avoid line mixing can have a detrimental effect on retrieval quality, compared with what one could achieve with the microwindow included and the line mixing properly accounted for.

Fig. 2 shows an example of line mixing in a Q-branch of CO_2 within the window used for retrievals of CCl_4. For a heavy molecule like CCl_4, there is only one possible window to employ in the retrievals. The strategy for minimizing line mixing effects for lighter molecules in ACE-FTS processing was a judicious selection of microwindows: limiting altitude ranges or discarding potential microwindows altogether if they were polluted with line mixing. With few (typically one or two) available microwindows for heavier molecules, there is no opportunity to employ this strategy.

In ACE-FTS version 3.0 (and earlier) processing, line mixing effects are ignored in the retrievals. For CCl_4 retrievals, this yields large residuals in the vicinity of the CO_2 Q-branch, as indicated by the circled portion of the residuals shown in Fig. 2. The contribution to the signal from CO_2 line mixing (evident in the shape of the enhanced residuals when line mixing is neglected) bears little resemblance to the broad CCl_4 spectral feature. The effects on CCl_4 retrievals of neglecting CO_2 line mixing are therefore not huge, but they are significant compared to the precision achievable with the ACE-FTS instrument, as reported previously in a study of a research version of ACE-FTS CCl_4 [24], where a systematic decrease of 3–5% in retrieved upper-tropospheric CCl_4 was observed in a set of tropical occultations when line mixing in the CO_2 Q-branch was taken into account.

The line mixing parameters for the CO_2 Q-branch derived from the ACE-FTS spectra are in rough agreement with previous studies [1], but with the significant difference in assumed temperature dependence and reference temperature, one would not expect close agreement. As before, the parameters derived in this analysis are not intended for future processing.

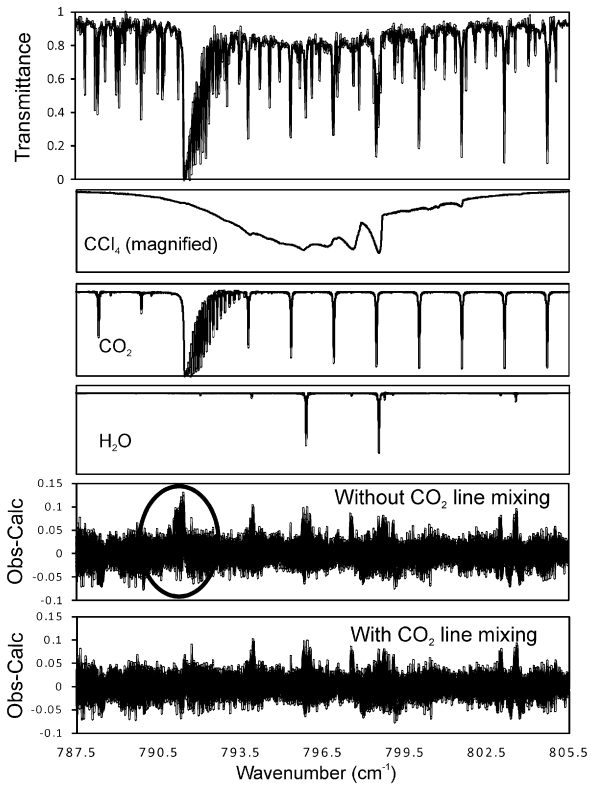

Fig. 2. Window region for the retrieval of CCl_4 for the ACE-FTS. The top panel shows the measured spectrum near 15 km for ss11613 (latitude 4°S, longitude 108°W, October 9, 2005). The three panels below that indicate the contributions to the spectrum from CCl_4, CO_2, and H_2O, respectively. The next panel shows the fitting residuals when line mixing in the CO_2 Q-branch is neglected, with enhanced residuals due to CO_2 line mixing circled, where the residuals for all measurements between 7 and 30 km (a total of 21 measurements) are included on a common plot. The bottom panel contains the fitting residuals when CO_2 line mixing is taken into account, where the line mixing parameters are determined from least-squares fitting of the ACE-FTS spectra.

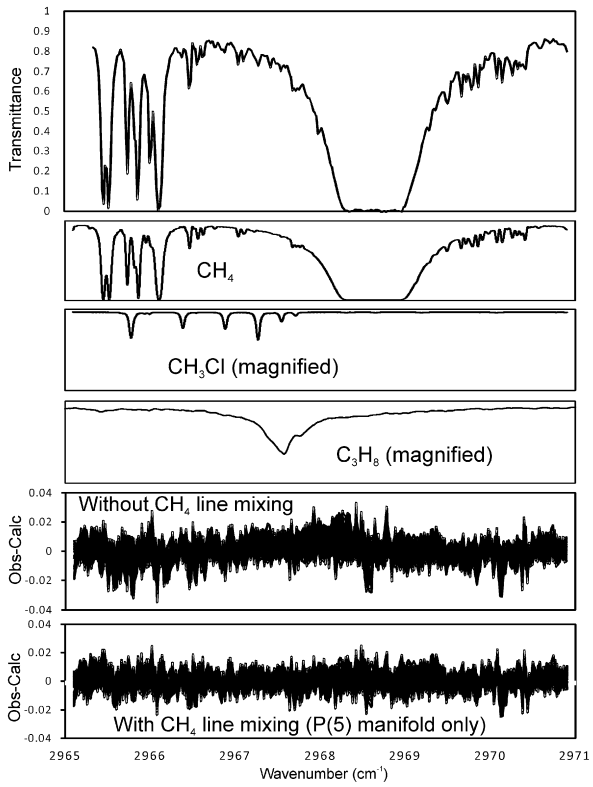

Fig. 3. ACE-FTS spectrum in the vicinity of a Q-branch for propane (C_3H_8). The top panel shows the measured spectrum near 15 km in sr10063 (latitude 38°S, longitude 160°E, June 25th, 2005). The next three panels show the contributions to the spectrum from CH_4, CH_3Cl, and C_3H_8, respectively. The next panel shows the fitting residuals with CH_4 line mixing neglected, where the residuals for all of the measurements in the occultation between 10 and 35 km (a total of 31 measurements) are shown on a common plot. The bottom panel shows the fitting residuals when line mixing is used for the CH_4 lines in the P(5) manifold of the ν_3 band, where the line mixing parameters are determined from least-squares fitting of the ACE-FTS spectra.

Note also the enhanced residuals in Fig. 2 in the vicinity of H_2O lines. This is a separate issue, a combination of neglecting speed dependence in the H_2O line shape and shortcomings in the ACE-FTS forward model for H_2O in the troposphere: the forward model performs calculations on a 1 km altitude grid, but H_2O VMR can change by a factor of two over the span of 1 km in the troposphere. Studies regarding the line shape of H_2O in ACE-FTS spectra are ongoing.

The best possibility for retrieving propane (C_3H_8) from the ACE-FTS spectra is a Q-branch near 2967.5 cm^{-1}. As seen in Fig. 3, this Q-branch resides near the P(5) manifold in the ν_3 band of CH_4. Line mixing in this manifold yields a relatively broad contribution to the spectrum that overlaps the location of the propane Q-branch, making it difficult to develop a retrieval procedure for the molecule. In Fig. 3, line mixing parameters were generated for the lines in the CH_4 P(5) manifold from the ACE-FTS spectra. If there were a weak signature of propane in this occultation, determining line mixing parameters from the ACE-FTS spectra would mask its presence. In order to search for propane in the ACE-FTS spectra, line mixing parameters for the P(5) manifold need to be generated from CH_4 laboratory spectra.

In Fig. 3, line mixing parameters were generated only for the P(5) manifold, although there are many other CH_4 lines in this region. Systematic features in the residuals indicate that there might be (relatively small) line mixing effects in at least some of these other CH_4 lines. In ACE-FTS version 3.0, information on CH_3Cl below 22 km comes exclusively from the relatively weak spectral features in this region. The broad spectral contribution from line mixing in the CH_4 P(5) manifold does not significantly affect the CH_3Cl retrievals, but neglected line mixing for other CH_4 lines in the region may have some influence. Investigations into this possibility also await analysis of the CH_4 laboratory spectra.

4. Line mixing and speed dependence combined

The Voigt function assumes that all molecules in a given quantum state experience the same pressure broadening regardless of velocity. For a range of pressures encountered

in Earth's atmosphere, this assumption can break down for light molecules such as CH_4 with heavier collision partners like O_2 and N_2. One strategy for modeling speed dependence in the line shape is to introduce a term in the pressure broadening half width that is proportional to the square of the velocity [25], thereby correlating pressure broadening with Doppler broadening.

In principle, collision-induced line mixing effects should also be speed dependent, because the cross section for collisions increases as molecule's velocity increases. A rigorous treatment of the effect would involve modeling the speed dependence of the line mixing (i.e., deducing a function of velocity that accurately depicted the variation of the line mixing parameter) and then integrating (or performing a weighted average) over the Maxwell–Boltzmann velocity distribution. However, the calculation complexity of the rigorous treatment would not be conducive to rapid calculations typically required for atmospheric retrievals.

Thus following the approach in Pine and Gabard [5], we neglect speed dependence in the line mixing and introduce a simple empirical extension of the first order Rosenkranz approximation to include the effects of speed dependence:

$$g_{SD,LM} = \frac{\sqrt{\ln 2/\pi}}{\gamma_D}\mathbf{Re}[(1-iY)I_{SD}], \tag{10}$$

where the subscripts SD and LM refer to speed dependence and line mixing, respectively, I_{SD} is the speed dependent Voigt function, and Y is the usual coupling coefficient from the Rosenkranz first order approximation.

From Boone et al. [26], I_{SD} can be calculated from:

$$I_{SD} = e^{z_1^2}\mathrm{erfc}(z_1) - e^{z_2^2}\mathrm{erfc}(z_2), \tag{11}$$

which is the difference between two terms with the form of the complex probability function $w(z)$, as defined in Eq. (6). The complex variables z_1 and z_2 are calculated as follows:

$$z_1 = \frac{1}{\sqrt{2}}\sqrt{\sqrt{(\delta+\alpha)^2+\beta^2}+\delta+\alpha} + \frac{i\ \mathrm{sign}(\beta)}{\sqrt{2}}\sqrt{\sqrt{(\delta+\alpha)^2+\beta^2}-\delta-\alpha}-\sqrt{\delta}, \text{ and}$$
$$z_2 = z_1 + 2\sqrt{\delta}, \tag{12}$$

where $\mathrm{sign}(\beta)$ indicates the sign of β (+ if β is positive, − if it is negative), and

$$\alpha = \frac{\gamma_L}{\gamma_2} - \frac{3}{2}, \beta = \frac{\omega-\omega_o+\eta}{\gamma_2}, \text{ and } \delta = \frac{1}{4\ln 2}\frac{\gamma_D^2}{\gamma_2^2}, \tag{13}$$

where γ_L, ω, ω_o, η, and γ_D are defined as for the Voigt function. The quantity γ_2 is a parameter that represents the speed dependence of the pressure broadening half width, arising from an assumed quadratic variation of pressure broadening with velocity, v [25]

$$\gamma(v) = \gamma_L + \gamma_2\left[\left(\frac{v}{v_o}\right)^2 - \frac{3}{2}\right], \tag{14}$$

where v_o is the most probable speed of the molecule within its Maxwell–Boltzmann velocity distribution

$$v_o = \sqrt{\frac{2kT}{m}}, \tag{15}$$

with the variables k, T, and m as defined previously.

In Boone et al. [26], it was suggested that the Kuntz implementation of the Humlicek algorithm [18,19] be used to calculate the real components of the two terms in Eq. (11). Similarly, the Humlicek approach can be used to calculate the imaginary component of I_{SD}, employing the expressions in the Appendix of this paper to calculate the imaginary components of the two terms in Eq. (11).

An investigation was performed on the accuracy of using the Humlicek approach for calculating the speed dependent Voigt function described above. The analytical calculation for the speed dependent Voigt was compared with the results of a "brute-force" numerical integration of the original integral used to derive the analytical expressions [26]. The brute force method employed 200 million points in the numerical integration to achieve accuracies of better than 1 part in a million.

Recall that the Humlicek approach breaks the calculation into four different regions: a far-wing region (Region 1), a near-wing region (Region 2), and two regions near the center of the line (Regions 3 and 4), although the nature of the two terms in Eq. (11) is such that Region 4 will seldom be encountered under normal atmospheric conditions. There are spikes in the errors from the analytical calculation when the two terms in Eq. (11) are situated in different Humlicek regions, in both the real and imaginary components. For typical atmospheric conditions, these errors are small, the order of 3 parts in 10^5 of the peak magnitude in the real component. Errors of this magnitude would likely only be noticeable for strongly saturated lines, where the wings of the lines are magnified. For optimal performance, one should ensure the calculations employed for the two terms in Eq. (11) are in the same region. If one term is in Region 1 and the other in Region 2, calculate both terms using the expressions associated with Region 2. Similarly, if the two terms span Regions 2 and 3, employ the expressions from Region 3 for both terms.

In Region 2 near the boundary with Region 3 (i.e., near $|x|+y=5.5$), there is a sharp increase in the errors associated with the analytical calculation, in both the real and imaginary components but larger in magnitude in the real component. In this vicinity, the two functions in Eq. (11) are of similar magnitude and the errors on each individual term increases as the calculation approaches Region 3. Differencing two terms of similar magnitude magnifies the error. Once again, the errors are relatively small, a maximum of about 3 parts in 10^5 of the peak magnitude in the real component. Changing the boundary between Regions 2 and 3 to $|x|+y=6.0$ reduces the maximum error by about a factor of three. Thus, when calculating the speed dependent Voigt function from the Humlicek approach, we recommend the use of this alternate boundary between Regions 2 and 3.

An example in the ACE-FTS spectrum where both line mixing and speed dependence is required is shown in Fig. 4. There is a Q-branch of acetone in this window, and residuals from the CH_4 lines were contaminating the acetone retrieval results. The combination of line mixing and speed dependence yields better residuals compared to line mixing or speed dependence alone, thereby improving retrievals for acetone from this window. Once again, spectroscopic parameters for this line shape were generated from analysis of the ACE-FTS spectra. A final set of parameters will be derived from the analysis of CH_4 laboratory spectra.

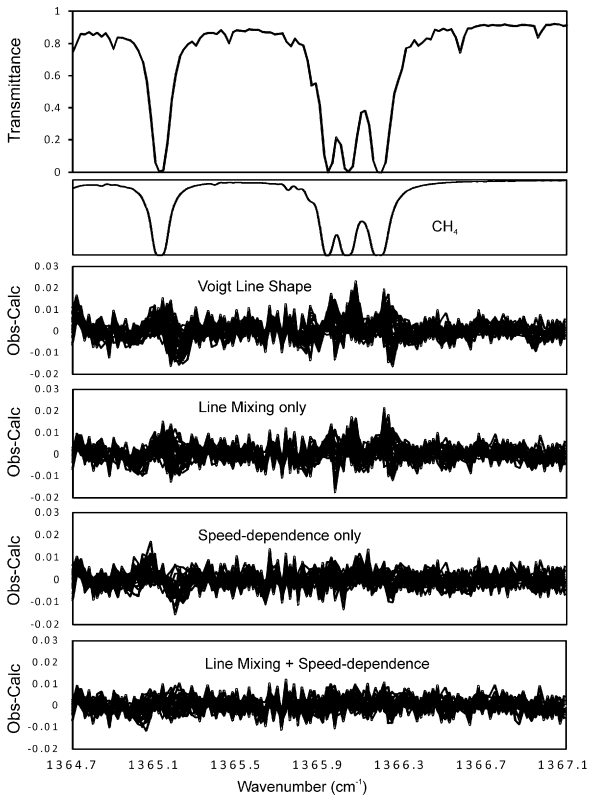

Fig. 4. ACE-FTS spectrum in the vicinity of a Q-branch of acetone (CH_3COCH_3). The top panel shows the measured spectrum near 15 km in sr10063 (latitude 38°S, longitude 160°E, June 25th, 2005). The panel below that shows the contribution to the spectrum from CH_4. Below that are the residuals when the Voigt line shape is used, where the residuals for all of the measurements in the occultation between 8 and 25 km (a total of 28 measurements) are shown on a common plot. The next panel shows the residuals when line mixing (but no speed dependence) is used for the strong CH_4 lines in the window, and the panel below that has the fitting residuals when speed dependence (but no line mixing) is used for the CH_4 lines. The bottom panel plots the residuals when a combination of line mixing and speed dependence is used for the CH_4 lines.

5. Discussion and conclusions

Failing to account for line mixing in the ACE-FTS spectra serves as an impediment to (1) retrieving new molecules from the measurements and (2) improving the accuracies for some existing retrievals. Work is underway to include the effects of line mixing (along with speed dependence) in the analysis of ACE-FTS spectra to more fully exploit instrument's very high signal-to-noise ratio.

Efficient analytical expressions for calculating the imaginary component of the Voigt function, required for the Rosenkranz first order approximation, are presented in the Appendix of this paper and serve as a complement to the analytical expressions for the real component provided in the paper by Kuntz [18,19].

A simple empirical extension of the Rosenkranz first order approximation permits a combination of line mixing and speed dependence, which appears to be necessary for proper treatment of some CH_4 lines in ACE-FTS spectra.

It is important to point out that the line shapes presented here do not strive for the truest physical model or the most accurate calculation approach. The primary goal is to have analytical line shapes that provide significant improvements in fitting residuals over the Voigt function (and therefore improve retrieval results) with the minimum possible increase in calculation complexity compared to the Voigt function. These line shapes are intended to be simple and efficient to calculate, geared toward line-by-line forward model calculations for atmospheric remote sensing. At their most complicated, with the combination of line mixing and speed dependence, the calculation involves determining four terms with computational requirements equivalent to a single calculation for the Voigt function, although similarities between input quantities for the different terms (see Eq. (12)) offer some possibility of optimizing the calculations.

As mentioned previously, the Rosenkranz first order approximation is not as accurate as an alternative approach for the treatment of line mixing that makes use of the relaxation matrix [5,6]. However, the approach involving the relaxation matrix is much less efficient, diagonalizing a matrix at every spectral point. The approach described in this paper using the Rosenkranz first order approximation is more compatible with line-by-line calculations, requiring one extra column in line-by-line spectral parameter databases such as HITRAN [16] for the coupling coefficient, Y, and likely a second column for a parameter describing the temperature dependence of Y.

Note that there exists a "hybrid" approach, where elements of the relaxation matrix are used to generate a coupling coefficient Y for the Rosenkranz first order approximation [27]. This avoids the need to diagonalize the matrix at every spectral point, enforces proper behavior in the wings of the lines (by ensuring that the weighted sum of particular matrix elements sum to zero [27]), and provides a better temperature dependence than using either the overly simple form in Eq. (9) or more complicated expressions for temperature dependence where parameters are excessively correlated [1]. This hybrid approach is not compatible with a line-by-line database; it requires external software for calculating the coupling coefficients.

The biggest stumbling block to using line shapes other than the Voigt function is the lack of spectroscopic constants for new parameters introduced by the non-Voigt line shape, as well as knowledge of changes in existing parameters from correlations between the new and existing parameters (see, e.g., D'Eu et al. [28]). To that end, CH_4 laboratory spectra are being measured and will be used to generate spectroscopic constants for use in the analysis of ACE-FTS spectra.

A collection of FORTRAN subroutines used for calculating the line mixing and the speed dependence plus line mixing profiles described here is available as a supplement to this paper.

Acknowledgments

Funding was provided by the Canadian Space Agency and the Natural Sciences and Engineering Research Council (NSERC) of Canada. Some funding was also provided by the UK Natural Environment Research Council.

Appendix

Region 1: $|x|+y>15$

$$a_1 = -0.2820948 + 0.5641896y^2$$

$$b_1 = 0.5641896$$

$$a_2 = 0.25 + y^2 + y^4$$

$$b_2 = -1.0 + 2y^2$$

$$L(x,y) = \frac{a_1 x + b_1 x^3}{a_2 + b_2 x^2 + x^4}.$$

Region 2: $\alpha < |x|+y < 15$, α=5.5 for Voigt or α=6.0 for speed dependent Voigt (SDV)

$$a_3 = -1.0578555 + 2.9619954y^2 + 2.5388532y^4 + 0.5641896y^6$$

$$b_3 = 4.6545642 - 0.5641896y^2 + 1.6925688y^4$$

$$c_3 = -3.1030428 + 1.6925688y^2$$

$$d_3 = 0.5641896$$

$$a_4 = 0.5625 + 4.5y^2 + 10.5y^4 + 6.0y^6 + y^8$$

$$b_4 = -4.5 + 9.0y^2 + 6.0y^4 + 4.0y^6$$

$$c_4 = 10.5 - 6.0y^2 + 6.0y^4$$

$$d_4 = -6.0 + 4.0y^2$$

$$L(x,y) = \frac{a_3 x + b_3 x^3 + c_3 x^5 + d_3 x^7}{a_4 + b_4 x^2 + c_4 x^4 + d_4 x^6 + x^8}.$$

Region 3: $|x|+y<\alpha$ and $y > 0.195|x| - 0.176$, α=5.5 (Voigt) or α=6.0 (SDV)

$$a_5 = 307.0522 + 900.8651y + 1215.616y^2 + 988.17457y^3 + 534.07725y^4 + 196.836y^5 + 48.97184y^6 + 7.557974y^7 + 0.5642236y^8$$

$$b_5 = 33.630785 + 178.55242y + 284.30395y^2 + 231.99739y^3 + 99.056246y^4 + 22.673922y^5 + 2.2568944y^6$$

$$c_5 = 14.1547 + 35.161375y + 51.196966y^2 + 22.673922y^3 + 3.3853416y^4$$

$$d_5 = 1.1125621 + 7.557974y + 2.2568944y^2$$

$$e_5 = 0.5642236$$

$$a_6 = 272.102 + 1280.83y + 2802.87y^2 + 3764.97y^3 + 3447.63y^4 + 2256.98y^5 + 1074.41y^6 + 369.199y^7 + 88.2674y^8 + 13.3988y^9 + y^{10}$$

$$b_6 = 211.678 + 902.306y + 1758.34y^2 + 2037.31y^3 + 1549.68y^4 + 793.427y^5 + 266.299y^6 + 53.5952y^7 + 5.0y^8$$

$$c_6 = 78.866 + 308.186y + 497.302y^2 + 479.258y^3 + 269.292y^4 + 80.3928y^5 + 10.0y^6$$

$$d_6 = 22.0353 + 55.0293y + 92.7586y^2 + 53.5952y^3 + 10.0y^4$$

$$e_6 = 1.49645 + 13.3988y + 5.0y^2$$

$$L(x,y) = \frac{a_5 x + b_5 x^3 + c_5 x^5 + d_5 x^7 + e_5 x^9}{a_6 + b_6 x^2 + c_6 x^4 + d_6 x^6 + e_6 x^8 + x^{10}}.$$

Region 4: $|x|+y<\alpha$ and $y < 0.195|x| - 0.176$, α=5.5 (Voigt) or α=6.0 (SDV)

$$a_7 = -1.1602757e9 - 5.6050464e8y^2 + 6.5152333e8y^4 - 2.6389408e8y^6 + 6.31771e7y^8 - 1.6984609e7y^{10} + 1231645.5y^{12} - 610622.y^{14} + 23586.527y^{16} - 8009.0976y^{18} + 622.05559y^{20} - 77.05345y^{22} + 2.922644y^{24} - 0.56419y^{26}$$

$$b_7 = -9.8660434e8 + 9.85361e8y^2 + 2.4715686e8y^4 - 2.7016652e8y^6 + 1.4067656e8y^8 - 4073816.1y^{10} + 7528830.4y^{12} - 84607.61y^{14} + 49883.805y^{16} - 2198.8554y^{18} - 271.20157y^{20} + 29.789641y^{22} - 7.33447y^{24}$$

$$c_7 = -4.5666204e8 + 8.0698521e8y^2 - 2.942619e8y^4 - 9.9622353e7y^6 - 5569648.0y^8 - 3.3289558e7y^{10} + 900010.2y^{12} + 153467.79y^{14} - 26538.547y^{16} + 953.655y^{18} + 134.79153y^{20} - 44.00682y^{22}$$

$$d_7 = -1.5357482e8 + 2.9187633e8y^2 - 2.0446691e8y^4 + 4.1501295e7y^6 + 2.4620116e7y^8 + 1931143.3y^{10} - 18668.18y^{12} - 72520.91y^{14} + 8073.149y^{16} + 352.4668y^{18} - 161.3582y^{20}$$

$$e_7 = -4.0816819e7 + 8.6482898e7y^2 - 2.293025e7y^4 + 3.83112e7y^6 - 4681421.0y^8 - 9347168.0y^{10} - 79902.49y^{12} + 23137.06y^{14} + 575.167y^{16} - 403.395y^{18}$$

$$f_7 = -9694631.9 + 7723590.7y^2 - 2.3818001e7y^4 - 2240400.3y^6 - 1002996.0y^8 - 8821.0y^{10} + 37371.88y^{12} + 571.647y^{14} - 726.113y^{16}$$

$$g_7 = -1684097.5 + 3599154.6y^2 - 576053.88y^4 - 303568.92y^6 + 66212.07y^8 + 37544.8y^{10} + 260.197y^{12} - 968.15y^{14}$$

$$h_7 = -320772.08 + 234416.52y^2 + 98079.06y^4 + 66431.22y^6 + 23507.63y^8 - 125.59y^{10} - 968.15y^{12}$$

$$o_7 = -40649.182 + 45251.326y^2 + 25338.301y^4 + 8381.969y^6 - 296.38y^8 - 726.113y^{10}$$

$$p_7 = -5860.6757 + 2269.1863y^2 + 1097.7707y^4 - 228.5628y^6 - 403.3958y^8$$

$$q_7 = -571.6872 - 234.14331y^2 - 97.62033y^4 - 161.35834y^6$$

$$r_7 = -72.935866 - 23.03124y^2 - 44.00682y^4$$

$$s_7 = -2.359444 - 7.33447y^2$$

$$t_7 = -0.56419$$

$$\begin{aligned} a_8 = {} & 1.02827e9 - 1.5599e9y^2 + 1.17022e9y^4 - 5.79099e8y^6 \\ & + 2.11107e8y^8 - 6.11148e7y^{10} \\ & + 1.44648e7y^{12} - 2857210.0y^{14} + 483737.0y^{16} \\ & - 70946.1y^{18} + 9504.65y^{20} - 955.194y^{22} \\ & + 126.532y^{24} - 3.68288y^{26} + y^{28} \end{aligned}$$

$$\begin{aligned} b_8 = {} & 1.5599e9 - 2.28855e9y^2 + 1.66421e9y^4 \\ & - 7.5383e8y^6 + 2.89676e8y^8 - 7.01358e7y^{10} \\ & + 1.39465e7y^{12} - 2849540.0y^{14} + 498334.0y^{16} \\ & - 55600.0y^{18} + 3058.26y^{20} + 533.254y^{22} \\ & - 40.5117y^{24} + 14.0y^{26} \end{aligned}$$

$$\begin{aligned} c_8 = {} & 1.17022e9 - 1.66421e9y^2 + 1.06002e9y^4 \\ & - 6.60077e8y^6 + 6.33497e7y^8 - 4.60396e7y^{10} \\ & + 1.4841e7y^{12} - 1063520.0y^{14} - 217801.0y^{16} \\ & + 48153.3y^{18} - 1500.17y^{20} - 198.875y^{22} + 91.0y^{24} \end{aligned}$$

$$\begin{aligned} d_8 = {} & 5.79099e8 - 7.5383e8y^2 + 6.60077e8y^4 \\ & + 5.40371e7y^6 + 1.99846e8y^8 - 6876550.0y^{10} \\ & - 6890020.0y^{12} + 280427.y^{14} + 161461.y^{16} \\ & - 16493.7y^{18} - 567.163y^{20} + 364.0y^{22} \end{aligned}$$

$$\begin{aligned} e_8 = {} & 2.11107e8 - 2.89676e8y^2 + 6.33497e7y^4 \\ & - 1.99846e8y^6 - 5.01017e7y^8 - 5257220.0y^{10} \\ & + 1954700.0y^{12} + 240373.0y^{14} - 55582.0y^{16} \\ & - 1012.79y^{18} + 1001.0y^{20} \end{aligned}$$

$$\begin{aligned} f_8 = {} & 6.11148e7 - 7.01358e7y^2 + 4.60396e7y^4 \\ & - 6876550.0y^6 + 5257220.0y^8 + 3043160.0y^{10} \\ & + 123052.0y^{12} - 106663.0y^{14} - 1093.81y^{16} + 2002.0y^{18} \end{aligned}$$

$$\begin{aligned} g_8 = {} & 1.44648e7 - 1.39465e7y^2 + 1.4841e7y^4 \\ & + 6890020.0y^6 + 1954700.0y^8 - 123052.0y^{10} \\ & - 131336.5y^{12} - 486.14y^{14} + 3003.0y^{16} \end{aligned}$$

$$\begin{aligned} h_8 = {} & 2857210.0 - 2849550.0y^2 + 1063520.0y^4 \\ & + 280427.0y^6 - 240373.0y^8 - 106663.0y^{10} \\ & + 486.14y^{12} + 3432.0y^{14} \end{aligned}$$

$$\begin{aligned} o_8 = {} & 483737.0 - 498334.0y^2 - 217801.0y^4 \\ & - 161461.0y^6 - 55582.0y^8 + 1093.81y^{10} + 3003.0y^{12} \end{aligned}$$

$$\begin{aligned} p_8 = {} & 70946.1 - 55600.0y^2 - 48153.3y^4 \\ & - 16493.7y^6 + 1012.79y^8 + 2002.0y^{10} \end{aligned}$$

$$q_8 = 9504.65 - 3058.26y^2 - 1500.17y^4 + 567.163y^6 + 1001.0y^8$$

$$r_8 = 955.194 + 533.254y^2 + 198.875y^4 + 364.0y^6$$

$$s_8 = 126.532 + 40.5117y^2 + 91.0y^4$$

$$t_8 = 3.68288 + 14.0y^2$$

$$\begin{aligned} L(x,y) = {} & e^{x^2-y^2}\sin(2xy) \\ & - \frac{a_7x + b_7x^3 + c_7x^5 + d_7x^7 + e_7x^9 + f_7x^{11} + g_7x^{13} + h_7x^{15}}{a_8 + b_8x^2 + c_8x^4 + d_8x^6 + e_8x^8 + f_8x^{10} + g_8x^{12} + h_8x^{14}} \\ & \cdots \frac{+ o_7x^{17} + p_7x^{19} + q_7x^{21} + r_7x^{23} + s_7x^{25} + t_7x^{27}}{+ o_8x^{16} + p_8x^{18} + q_8x^{20} + r_8x^{22} + s_8x^{24} + t_8x^{26} + x^{28}}. \end{aligned}$$

Appendix B. Supporting information

Supplementary data associated with this article can be found in the online version at doi:10.1016/j.jqsrt.2010.11.013.

References

[1] Strow LL, Tobin DC, Hannon SE. A compilation of first-order line mixing coefficients for CO_2 Q-branches. J Quant Spectrosc Radiat Transfer 1994;52:281–94.

[2] Hartmann J-M, Tran H, Toon GC. Influence of line mixing on the retrievals of atmospheric CO_2 from spectra in the 1.6 and 2.1 μm regions. Atmos Chem Phys 2009;9:7303–12.

[3] Mondelain D, Payan S, Deng W, Camy-Peyret C, Hurtmans D, Mantz AW. Measurement of the temperature dependence of line mixing and pressure broadening parameters between 296 and 90 K in the ν_3 band of $^{12}CH_4$ and their influence on atmospheric methane retrievals. J Mol Spectrosc 2007;244:130–7.

[4] Pine AS. N_2 and Ar broadening and line mixing in the P and R branches of the ν_3 band of CH_4. J Quant Spectrosc Radiat Transfer 1997;57:157–76.

[5] Pine AS, Gabard T. Speed-dependent broadening and line mixing in CH_4 perturbed by Ar and N_2 from multispectrum fits. J Quant Spectrosc Radiat Transfer 2000;66:69–92.

[6] Smith MAH, Benner DC, Predio-Cross A, Malathy Devi V. Multispectrum analysis of $^{12}CH_4$ in the ν_4 band:I. Air-broadened halfwidths, pressure-induced shifts, temperature dependences and line mixing. J Quant Spectrosc Radiat Transfer 2009;110:639–53.

[7] Brown LR, Benner DC, Malathy Devi V, Smith MAH, Toth RA. Line mixing in self- and foreign-broadened water vapor at 6 μm. J Mol Struct 2005;742:111–22.

[8] Rodrigues R, De Natale P, Di Lonardo G, Hartmann J-M. Line-mixing effects in the rotational ^rQ-branches of $^{16}O_3$ perturbed by N_2 and O_2. J Mol Spectrosc 1996;175:429–40.

[9] Tran H, Rohart F, Boone C, Eremenko M, Hase F, Bernath P, et al. Non-Voigt line shape effects on retrievals of atmospheric ozone: collisionally isolated lines. J Quant Spectrosc Radiat Transfer 2010;111:2012–20.

[10] Brault JW, Brown LR, Chackerian Jr C, Freedman R, Predoi-Cross A, Pine AS. Self-broadened $^{12}C^{16}O$ line shapes in the $v=2\leftarrow0$ band. J Mol Spectrosc 2003;222:220–39.

[11] Hartmann J-M, Bouanich J-P, Jucks KW, Blanquet G, Walrand J, Bermejo D, et al. Line-mixing effects in N_2O Q-branches: model, laboratory, and atmospheric spectra. J Chem Phys 1999;110:1959–68.

[12] Frichot F, Lacome N, Hartmann J-M. Pressure and temperature dependences of absorption in the ν_5 $^RQ_0$ branch of CH_3Cl in N_2:measurements and modeling. J Mol Spectrosc 1996;178:52–8.

[13] Tran H, Jacquemart D, Mandin JY, Lacome N. Line mixing in the ν_6 Q-branches of self-and nitrogen-broadened methyl bromide. J Quant Spectros Radiat Transfer 2008;109:119–31.

[14] Hartmann J-M, Boulet C, Robert D. Collisional effects on molecular spectra laboratory experiments and models, consequences for applications. Amsterdam: Elsevier; 2008.

[15] Bernath PF, McElroy CT, Abrams MC, Boone CD, Butler M, Camy-Peyret C, et al. Atmospheric Chemistry Experiment (ACE): mission overview. Geophys Res Lett 2005;32:L15S01.

[16] Rothman LS, Gordon IE, Barbe A, Benner DC, Bernath PF, Birk M, et al. The HITRAN 2008 molecular spectroscopic database. J Quant Spectrosc Radiat Transfer 2009;110:533–72.

[17] Humlicek J. Optimized computation of the Voigt and complex probability functions. J Quant Spectrosc Radiat Transfer 1982;27:437–44.

[18] Kuntz M. A new implementation of the Humlicek algorithm for the calculation of the Voigt profile function. J Quant Spectrosc Radiat Transfer 1997;57:819–24.

[19] Ruyten W. Comment on a new implementation of the Humlicek algorithm for the calculation of the Voigt profile function by M. Kuntz

[JQSRT 57(6) (1997) 819–824]. J Quant Spectrosc Radiat Transfer 2004;86:231–3.
[20] Schreier F. The Voigt and complex error function: a comparison of computational methods. J Quant Spectrosc Radiat Transfer 1992;48: 743–62.
[21] Rosenkranz PW. Shape of the 5 mm oxygen band in the atmosphere. IEEE Trans Antennas Propag 1975;AP-23:498–506.
[22] Wells RJ. Rapid approximation to the Voigt/Faddeeva function and its derivatives. J Quant Spectrosc Radiat Transfer 1999;62:29–48.
[23] Boone CD, Nassar R, Walker KA, Rochon Y, McLeod SD, Rinsland CP, et al. Retrievals for the Atmospheric Chemistry Experiment Fourier-transform spectrometer. Appl Opt 2005;44:7218–31.
[24] Allen NDC, Bernath PF, Boone CD, Chipperfield MP, Fu D, Manney GL, et al. Global carbon tetrachloride distributions obtained from the atmospheric chemistry experiment (ACE). Atmos Chem Phys 2009;9: 7449–59.
[25] Rohart F, Colmont J-M, Wlodarczak G, Bouanich J-P. N_2- and O_2-broadening coefficients and profiles for millimeter lines of $^{14}N_2O$. J Mol Spectrosc 2003;222:159–71.
[26] Boone CD, Walker KA, Bernath PF. Speed-dependent Voigt profile for water vapour ininfrared remote sensing applications. J Quant Spectrosc Radiat Transfer 2007;105:525–32.
[27] Niro F, Jucks KW, Hartmann J-M. Spectra calculations in central and wing regions of CO_2 IR bands between 10 and 20 μm, IV: software and database for the computation of atmospheric spectra. J Quant Spectrosc Radiat Transfer 2005;95:469–81.
[28] D'Eu J-F, Lemoine B, Rohart F. Infrared HCN lineshapes as a test of Galatry and speed-dependent Voigt profiles. J Mol Spectrosc 2002;212:96–110.